Aging and Disease
www.aginganddisease.org
Early access date: January 29, 2026
http://dx.doi.org/10.14336/AD.2025.1249

Original Article

TRF2 Upregulates Protein Phosphatase 2A Subunit PPP2R2C to Attenuate DNA Damage Response at Telomeres and Pericentromeres Upon Replicative Stress

Xiuyun Zhai[1,2#], Cuicui Wang[1,2,5#], Yilin Ying[1,2#], Waiian Leong[1,2], Lianxiang Chen[1,2], Bohua Wei[1,2], Xiaojiao Cheng[6], Sheng Huang[1,2], Qiaowen Chen[1,2], Yiming Lu[1,2], Eric Gilson[2,3,4*], Jing Ye[1,2*]

[1]Department of Geriatrics, Medical center on Aging of Shanghai Ruijin Hospital, Shanghai Jiao Tong University School of Medicine, Shanghai, China. [2]International Laboratory in Cancer, Aging and Hematology, Shanghai Jiao Tong University School of Medicine/Ruijin Hospital/CNRS/Inserm/Côte d'Azur University, Shanghai, China. [3]Université Côte d'Azur, CNRS, INSERM, IRCAN, Medical School of Nice, Nice, France. [4]Department of Genetics, CHU, Nice, France. [5]Department of Emergency, Xinhua Hospital, Shanghai Jiao Tong University School of Medicine, Shanghai, China. [6]Department of Oncology, State Key Laboratory of Systems Medicine for Cancer, Renji Hospital, Shanghai Jiao Tong University School of Medicine, Shanghai, China

[Received October 7, 2025; Revised December 26, 2025; Accepted December 29, 2025]

ABSTRACT: Telomeres and pericentromeres are regions of heterochromatin that are difficult to replicate. Telomeric binding factor 2 (TRF2) is a key telomere protective protein that acts against DNA damage at telomeres and allows the progression of replication forks through telomere chromatin, a region with heterochromatin features that is difficult to replicate. TRF2 is also required at pericentromeres for proper replication elongation. Here, we show that TRF2 positively regulates the activity of protein phosphatase 2A (PP2A) by activating the expression of *PPP2R2C*, a gene encoding an isoform of the regulatory subunit of PP2A with particularly elevated expression in neuronal tissues. Mechanistically, we provide evidence that TRF2 binds to an intronic interstitial telomeric sequence (ITS) of *PPP2R2C* with transactivation activity. Moreover, PPP2R2C is recruited to telomeres and pericentromeres during S phase and during replicative stress where it attenuates the DNA damage response. Finally, we show that the TRF2-dependent regulation of PPP2R2C expression plays an important role in maintaining neurodevelopment in zebrafish. These results reveal a mechanism required for normal neurodevelopment by which TRF2 attenuates DNA damage by upregulating PPP2R2C, thereby stimulating PP2A activity at two regions difficult to replicate: telomeres and pericentromeres.

Keywords: DNA damage response, replicative stress, heterochromatin, PP2A, cellular senescence, aging

INTRODUCTION

The heterochromatin at telomeres and pericentromeres is considered as difficult-to-replicate regions leading to replication fork stalling. The integrity and function of telomeres are ensured through the telomerase [1] to avoid replicative erosion and the shelterin protein complex to prevent unwanted activation of the DNA damage response (DDR) at chromosome termini. Shelterin consists of six subunits: Telomeric Repeat binding Factor 1 and 2 (TRF1, TRF2), Protection of Telomeres 1 (POT1), TRF2- and TRF1-Interacting Nuclear protein 2 (TIN2), RAP1, and

***Correspondence should be addressed to:** Dr. Eric Gilson, Medical School of Nice, Université Côte d'Azur, France. E-mail: eric.gilson@unice.fr; Dr. Jing Ye, Department of Geriatrics, Medical center on Aging of Shanghai Ruijin Hospital, Shanghai, China, 200025. E-mail: yj11254@rjh.com.cn. #These authors contributed equally to this work.

TPP1. TRF2 is at the core of the shelterin protein complex, which protects against DDR activation by ataxia telangiectasia mutated kinase (ATM) [2]. In addition, TRF2 can form T-loops [3-7], which consist of G-rich repetitive DNA sequences with a single-stranded 3' overhang that invades the double-stranded region, shielding telomeric DNA from being unintentionally misrecognized as damaged DNA by the cell's repair machinery. TRF2 recruits Apollo protein to the telomere by its TRFH domain [8, 9]. TRF2 and Apollo work together with topoisomerase Top2α to reduce the topological pressure at replicating telomeres thus ensuring the smooth progress of replication forks [10]. Besides, TRF2 facilitates the progression of replication forks at the pericentromeres by recruiting the G4-resolving helicase RTEL1 [11]. In conclusion, TRF2 is crucial for the normal progression of the replication through telomeres and pericentromeres.

Recently, we have shown that TRF2 level is high in the brain and is progressively reduced during aging [12]. This suggests a specific function of TRF2 in the brain that is impaired during aging. TRF2 not only plays a protective role at telomeres and pericentromeres, but also binds to extratelomeric sites which are a subset of interstitial telomeric sequences (ITS) and satellite repeats [13]. Chromatin immunoprecipitation combined with high-throughput sequencing (ChIP-seq) analysis showed that most of the TRF2 bound-ITSs are localized close to neural genes [13, 14], reinforcing the hypothesis of neural specific functions of TRF2 [12].

PP2A is the main component of serine/threonine phosphatase in the brain, which is composed of core enzyme and regulatory subunit B. Core enzyme, a dimer including structural subunit A and catalytic subunit C, combines with regulatory subunit B to form different PP2A trimers [15]. Deregulation of PP2A core enzyme or its subunits has been implicated in the neuro-developmental and neurodegenerative diseases [16]. We have previously shown in zebrafish that PPP2R2C, a neural-specific isoform of the regulatory subunit of PP2A, protects against brain aging [17]. Moreover, decreased PPP2R2C expression induced PP2A inactivation in Alzheimer's disease (AD) and correlated with cognitive impairment in mouse model [18]. More interestingly, we have shown that the downregulation of TRF2 in zebrafish embryos repressed the expression of *ppp2r2c* [12, 13, 19].

In this study, we investigated possible relationships between TRF2 and PPP2R2C. We showed that the expression of PPP2R2C is not only positively regulated in zebrafish by TRF2 but also in human cells. We also provide evidence that PPP2R2C is localized at telomeres and pericentromeres during replication and avoids DNA damage in these difficult-to-replicate regions. Moreover, compromising the TRF2-PPP2R2C axis leads to DNA damage in neural tissues and abnormal neurodevelopment. These results point toward a novel mechanism of telomere and heterochromatin replicative damage by a TRF2-dependent activation of PP2A activity that is required for proper neurodevelopment.

MATERIALS AND METHODS

Cell lines, media and reagents

The fetal bovine serum for A375 cells is special for tetracycline (TC) regulatory system and addition of TC induces cells to overexpress TRF2. 293T, SH-SY5Y and U87-MG cells were obtained from cell resources center of Shanghai Life Research Institute. They were grown in Dulbecco's Modified Eagle Medium (DMEM) with 10% fetal bovine serum (FBS) at 37°C in a 5% CO_2 cell culture incubator. Primary glial cells were obtained as previously described [18]. MRC-5 cells were purchased from ATCC and cultured at 37 °C under 5% O_2 in DMEM supplemented with 10% FBS.

Zebrafish maintenance

Zebrafish used in these experiments were from the Tübingen (Tu) zebrafish strain. Zebrafish were raised and maintained as described previously [20]. All experiments concerning zebrafish were performed in accordance with the guidelines of the Animal Care and Use Committee of Shanghai Jiao Tong University. Zebrafish embryos were cultured in egg water at 28.5 °C.

Plasmids, siRNAs, lentivirus transfection and transient transfection

The human PPP2R2C cDNA was synthesized by Genscript Company, and its exact sequence is listed in Supplementary File S1. The PPP2R2C constructs for transfection were obtained by PCR cloning into a modified version of pWPIR to generate the full-length protein. To produce the lentiviruses, 8.6 μg of pWPIR-GFP vector expressing empty, PPP2R2C or pLKO.1 vector expressing TRF2 shRNA (TRCN0000004811, Sigma), PPP2R2C shRNA (TRCN0000006867, Sigma) or non-coding shRNA, 8.6 μg of pCMVΔR8.91 and 2.8 μg of pCMV-VSV-g were introduced into $5x10^6$ 293T cells through calcium phosphate mediated transfection (Promega E1200, USA). The infectious supernatant was harvested at 48 and 72 h after transfection and applied to infect target cells. The efficiency of infection was initially assessed by flow cytometry analysis of GFP expression 3 days or selected by 1 μg/ml puromycin 1 week after infection and finally confirmed by western blotting.

Human siTRF2 (L-003546), siTRF1 (L-010542), siPPP2R2C (L-019167), siCtrl (D-001810) were purchased from Dharmacon company. "L" (On-Target Plus SMARTpool) is a mixture of four siRNAs against the gene of interest. Transfections of siRNA were performed with Lipofectamine 2000 reagent (Invitrogen, 11668019) according to the manufacturer's protocol for 72 h.

Western Blotting

Protein lysates were prepared in the ice-cold lysis buffer containing 1X RIPA (Beyotime Biotechnology, China), 1 mM phenylmethylsulfonyl fluoride (PMSF, Beyotime Biotechnology), a protease inhibitor mixture (Roche Molecular Biochemical, Switzerland) and a phosphatase inhibitor cocktail (Roche Molecular Biochemical, Switzerland) for 5 min. The lysate was centrifuged at 12,000X g for 30 min at 4 °C and the supernatant fraction was used for western blot analysis. 30-50 μg of protein samples were subjected to 10% SDS–polyacrylamide gel electrophoresis. Next, proteins were transferred to polyvinylidene fluoride (PVDF) membranes (Millipore, USA) and blocked with 5% milk in TBST (0.1% Tween-20 in TBS) for 1 h at room temperature. The Hybridization of primary antibody were performed at 4 °C overnight. The membranes were washed by TBST three times and followed by incubating with corresponding second antibodies at 37 °C for 2 h. The images were detected by the ImageQuant LAS 4000 System (GE healthcare, UK). The antibodies used in this study are listed in Supplementary Table 1.

Reverse transcription quantitative polymerase chain reaction (RT-qPCR)

Gene expression levels were verified by RT-qPCR carried out in triplicate using cDNA from total RNA. RT-qPCR was used to determine the efficiency of siRNA or shRNA downregulation. Total RNA was extracted from cells with Trizol reagent (Invitrogen). Total RNA was synthesized into cDNA using RT-qPCR Kit (Takara) according to the manufacturer's protocol. qPCR was performed using a commercial SYBR® Green Kit (Tiangen). Primer sequences used in this study are listed in Supplementary Table 2.

PP2A phosphatase assay

Cells were lysed with 20 mM imidazole-HCl, 2 mM EDTA, 2 mM EGTA, 10 μg/mL aprotinin, 10 μg/mL leupeptin, 10 μg/mL antipain, 1 mM phenylmethyl-sulfonyl fluoride, 1 mM benzamidine at pH 7.0 and final concentration 1% of NP-40. The phosphatase PP2A activity was measured as described previously [17] by PP2A Immunoprecipitation Phosphatase Assay Kit (Millipore).

Chromatin immunoprecipitation (CHIP)

Cells were cross-linked for 10 min at room temperature with a final concentration of 1% formaldehyde and washed twice with ice-cold PBS. The formaldehyde was quenched with glycine (final concentration 0.125 M) and placed at room temperature for 5 min followed by washing twice with ice-cold PBS. The cells in ice-cold PBS were collected using a cell scraper and centrifuged at 5000 rpm at 4 °C for 5 min. After incubation for 20 min in cell lysis buffer (5 mM PIPES, 85 mM KCl, 0.5% NP-40, protease inhibitors), the pellets were resuspended and sonicated in nuclear lysis buffer (50 mM Tris, 10 mM EDTA, 1% SDS, protease inhibitors), using a Bioruptor sonicator, until the average fragment size reached 1000 bp. After centrifugation at 14000 rpm at 4 °C for 20 min, the supernatants were transferred and 20 μL of supernatant was left as input. The remaining supernatant was diluted 10-fold to reduce the following final concentration of the ChIP buffer (16.7 mM Tris, 167 mM NaCl, 1.2 mM EDTA, 1.1% Triton and 0.01% SDS). The precleared sonicates were incubated with Protein G Sepharose beads (GE Healthcare) pre-coated with 0.1% BSA at 4 °C for 2 h. The supernatants were collected and incubated overnight with the primary antibody. Protein G Sepharose beads were added for a further 2 h. The beads were washed with low-salt buffer (20 mM Tris, 150 mM NaCl, 2 mM EDTA, 1% Triton and 0.1% SDS), high-salt buffer (20 mM Tris, 500 mM NaCl, 2 mM EDTA, 1% Triton and 0.1% SDS), lithium wash buffer (10 mM Tris, 250 mM LiCl, 1 mM EDTA, 1% NP-40, 1% DOC) followed by TE buffer (10 mM Tris, 1 mM EDTA). Chromatin was eluted with a 1% SDS, 0.1 M NaHCO3 solution and cross-linking was reversed at 65 °C overnight. DNA was purified by proteinase K (50 μg/mL final concentration) for 2 h at 45 °C, followed by classic phenol-chloroform purification and ethanol precipitation steps. Antibodies against TRF2m (Imgenex 124A, mouse monoclonal) and total histone H3 (Abcam ab1791, rabbit polyclonal) were used.

Luciferase activity assay

The A375 cells were seeded in 6-well plates at a density of 2.5×10^5 cells per well and cultured for 24 h prior to transfection. Transfections were performed using Effectene Transfection Reagent (QIAGEN, 301427) with a total of 1 μg plasmid DNA per well for 48 h. This consisted of 500 ng of the firefly luciferase reporter plasmid (PGL4.20) and 500 ng of the Renilla luciferase internal control plasmid (pRL-TK), a 1:1 ratio optimized

for A375 cells based on the manufacturer's protocol (Promega Dual-Luciferase® Reporter Assay System, E1910) and our pre-experimental validation. Firefly luciferase activity was normalized to Renilla luciferase activity from pRL-TK to control for variations in transfection efficiency and cell viability.

Comet assay

For each condition, 7000 cells were pelleted and resuspended in 50 µL of 0.5% low melting point agarose dissolved in 1X PBS at 42 °C. The suspension was immediately laid onto a comet slide (4250-200-03, Trevigen). Agarose was allowed to solidify at 4 °C for 20 min. The comet slides were then immersed in prechilled lysis solution (2.5 M NaCl, 100 mM Na2EDTA, 10 mM Tris, 1% TritonX-100, pH=10.0) at 4 °C for 90 min in the dark. After this treatment, comet slides were placed in a horizontal electrophoresis unit and allowed to equilibrate in electrophoresis buffer for 5 min at 4 °C in the dark. The migration was then performed in 0.5X TBE buffer (pH=8) at 40 V for 20 min. Slides were then placed in ethanol (100%) for 30 min at 4 °C (slides can be stored for few days under these conditions). Slides were transferred into neutralization solution and followed by gradient alcohol dehydration (50%, 70%, 100%) at room temperature. Slides were then thoroughly air-dried and the DNA was stained with DAPI or YOYO-1 for 10 min.

Comet analysis was performed using the Tritek Comet Score freeware, which measures a wide range of densitometric parameters for each comet. The tail moment (= tail length × DNA in the tail / total DNA) was recorded for each comet (40-50 cells).

Immunofluorescence (IF) and Fluorescence in situ hybridization (FISH)

Cells on coverslips were fixed with 4% paraformaldehyde for 15 min, washed with 1X PBS for 5 min, three times, permeabilized in 0.5% Triton X-100 (in 1X PBS) for 30 min. The slides were blocked with 5% BSA for 2 h and stained with PPP2R2C, TRF2, 53BP1, γ-H2AX, RPA and p-ATM overnight at 4°C, washed three times with PBST (0.1% Triton X-100 in PBS), and incubated with secondary antibodies. The corresponding secondary antibodies were Alexa Fluor 555 goat anti-mouse antibody, Alexa Fluor 488 donkey anti-mouse antibody, Alexa Fluor 555 donkey anti-rabbit antibody, Alexa Fluor 488 goat anti-rabbit, which were incubated for 1 h at room temperature. The coverslips were washed three times with PBST, incubated in 4% paraformaldehyde for 10 min, dehydrated in increasing concentrations of ethanol for 5 min (70%, 95% and 100%). Hybridization of telomeric PNA probes $(CCCTAA)_3$ or SatIII PNA probes $(TTCCA)_4$ or Centromeric PNA probes (AAACTAGA CAGAAGCATT) (Panagene) was performed for at least 2 h at RT after a 3 min denaturation in 70% formamide, 10 mM Tris pH 7.2 and 1% blocking solution (Roche) at 80 °C. After that, the cells were washed in a 70% formamide, 10 mM Tris pH 7.2 solution for 30 min, followed by a solution containing 150 mM NaCl and 50 mM Tris pH 7.5 for 15 min. Finally, the cells were stained with 1X DAPI and preserved. Fluorescence was detected and imaged using a Leica SP8 confocal microscope. The antibodies used in this study are listed in Supplementary Table 1.

Cell cycle synchronization and treatment

For cell cycle synchronization, SH-SY5Y cells were treated with thymidine (2 mM, Sigma, T9250) for 19 h, followed by three washes with pre-warmed PBS and a 9 h culture in fresh medium. This was followed by a second thymidine (2 mM) block for 17 h, after which the cells were released into fresh medium. Replicative stress was induced with hydroxyurea (1.5 µM, Sangon Biotech, HB0528) and aphidicolin (300 nM, Sigma, A0781).

Flow Cytometry Analysis

At least $1x10^6$ cells per condition were grown onto dishes overnight before collection. Trypsinized cells were fixed with 70% ethanol (pre-cooled to -20 °C) dropwise while shaking and stored at 4 °C overnight or -20 °C for long-term storage. Next, cells were washed three times with PBS and incubated with RNase (100 µg/mL, Sangon Biotech, B600476), PI (50 µg/mL, Sangon Biotech, A601112) in PBS at 37 °C for 1 h before detection. The flow cytometry was performed using BD FACSCalibur.

EdU staining

EdU staining was performed in accordance with the protocol of Click-iT® EdU Imaging Kits (Invitrogen, C10340). Cells were grown onto glass coverslips at the desired density overnight before additional treatments. 293T and U87-MG cells were treated with EdU (10 µM) for 2 h before being fixed with 4% formaldehyde in PBS for 15 min at room temperature. The cells were washed with 3% BSA in PBS twice and permeabilized with 0.5% Triton X-100 in PBS at room temperature for 20 min. Next, the slides were washed with 3% BSA in PBS twice and added appropriate volume of Click-iT® reaction cocktail according to kit for 30 min at room temperature. After that, the cells were washed with 3% BSA in PBS twice. Following procedures refer to the steps after blocking in IF.

Proximity Ligation Assay (PLA)

The interaction between PPP2R2C and TRF2 was also detected by the proximity ligation assay kit Duolink® In Situ Red Starter Kit Mouse/Rabbit (Sigma, DUO92101). The PLA probe anti-rabbit plus binds to TRF2 antibody, whereas the PLA probe anti-mouse minus binds to the antibody against PPP2R2C, respectively. The Duolink proximity ligation assay secondary antibodies generate signals when two PLA probes have bound. Cells were fixed, permeabilized, blocked as the steps in IF and primary PPP2R2C and TRF2 antibodies were applied to the samples. Incubation was done overnight in a humidity chamber at 4 °C. Slides were washed three times in PBST (0.1% Triton X-100 in PBS) for 10 min. Duolink PLA probes detecting rabbit or mouse antibodies were diluted in the blocking agent at a ratio of 1:5 and applied to the slides followed by incubation for 1 h in a pre-heated humidity chamber at 37 °C. Unbound PLA probes were removed by washing twice with washing buffer A for 5 min. The samples were incubated with the ligation solution consisting of Duolink Ligation stock (1:5) and Duolink Ligase (1:40) diluted in high purity water for 30 min at 37 °C. The slides were washed two times by washing buffer A for 5 min. Next, the Duolink Amplification and Detection stock, diluted 1:5 by the addition of polymerase (1:80), was applied to the slides for 100 min. The slides were washed two times by washing buffer B for 10 min. Afterwards the slides were incubated with Duolink in Situ Mounting medium with DAPI. After the final washing steps the slides were dried and coverslips were mounted. Fluorescence was detected and imaged using a Leica SP8 confocal microscope. The antibodies used in this study are listed in Supplementary Table 1.

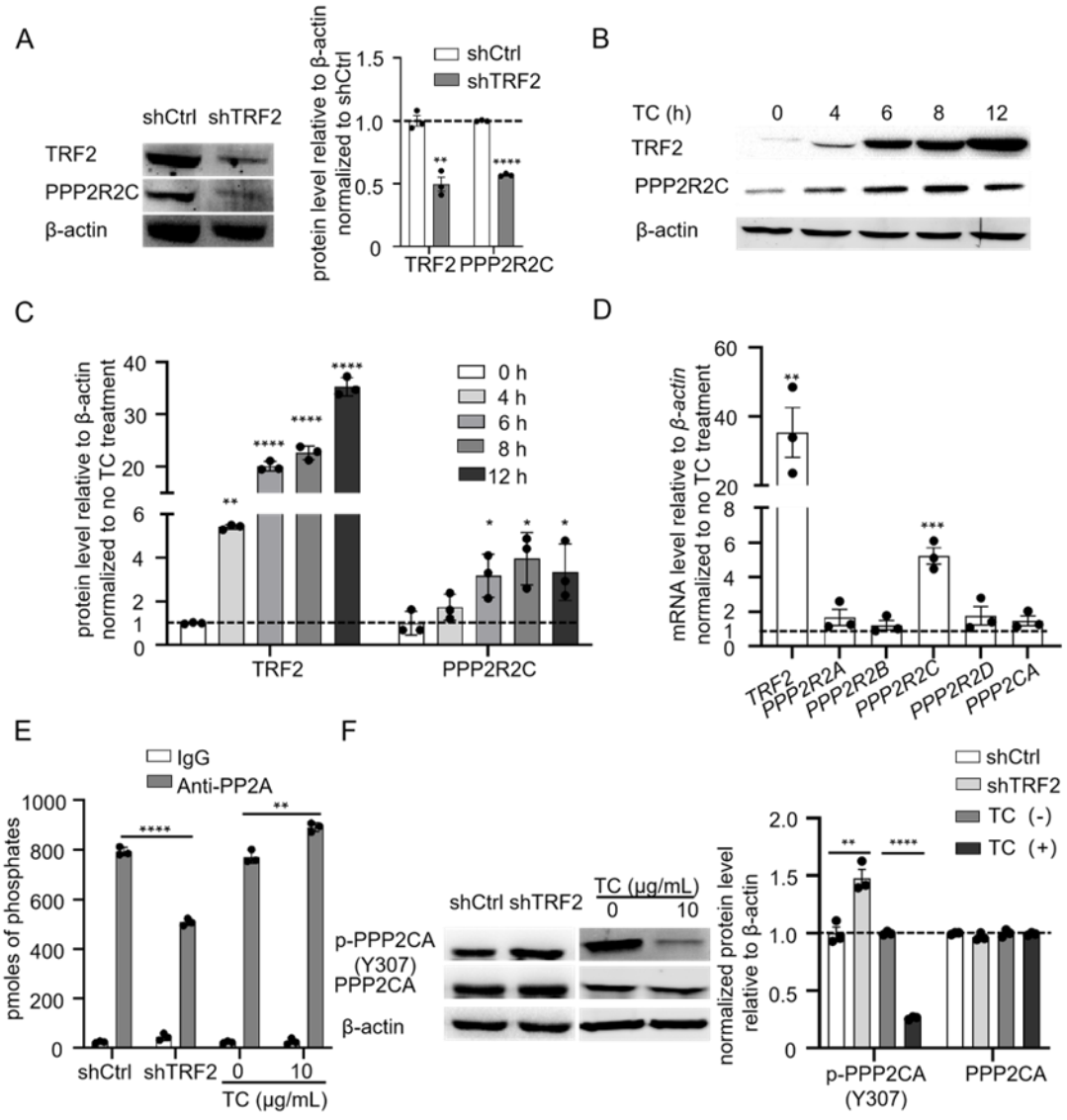

Figure 1. TRF2 Positively Regulates PPP2R2C Expression and Phosphatase Activity of PP2A. (A) Western blot (WB) analysis was performed on U87-MG cells infected with lentiviruses encoding scramble shRNA (shCtrl) and TRF2 mRNA-specific shRNA (shTRF2), respectively. Band intensities were relatively quantified via grayscale analysis with β-actin as the internal reference and normalized to the shCtrl group. **(B-C)** Representative WB images and grayscale quantification analysis of TRF2 and PPP2R2C protein levels were conducted in A375 cells treated with tetracycline (TC, concentration: 0.5 μg/mL) for different time periods to induce TRF2 overexpression. The protein levels of TRF2 and PPP2R2C were relatively quantified using β-actin as the internal reference and normalized to the group without TC treatment. **(D)** Reverse transcription quantitative polymerase chain reaction (RT-qPCR) analysis was carried out on A375 cells treated with TC (concentration: 100 μg/mL) for 12 hours to induce TRF2 overexpression. The mRNA levels of the target genes were relatively quantified with *β-actin* as the internal reference and normalized to the group without TC treatment. **(E)** PP2A phosphatase activity was measured in two groups of cells separately: one group was SH-SY5Y cells transfected with TRF2-targeting shRNA, and the other group was A375 cells treated with TC (concentration: 10 μg/mL) for 12 hours to induce TRF2 overexpression. **(F)** Immunoblot analysis and quantification were performed on two groups of cells: one group was SH-SY5Y cells transfected with scramble shRNA (shCtrl) or TRF2-specific shRNA, in which the protein levels of phosphorylated PPP2CA (at Y307 site, p-PPP2CA) and total PPP2CA were detected; the other group was A375 cells treated with indicated concentrations of TC for 12 hours to induce TRF2 overexpression, and the above-mentioned protein levels were also detected. All experimental data are presented as mean ± SEM (n=3). The unpaired two-tailed t-tests for (A), (D), (E), and (F), one-way ANOVA followed by Bonferroni's post hoc test for (C), *p < 0.05, **p < 0.01, ***p < 0.001, ****p < 0.0001.

Senescence-associated β-galactosidase

Senescence β-galactosidase Staining Kit (Beyotime) was used to detect senescence-associated β-galactosidase (SA-β-gal). The assays were performed in accordance with manufacturer's instructions. Images were collected using Zeiss A2 microscope.

Morpholino and mRNA synthesis for microinjection

Zebrafish *terfa* (5'-CTCGCAGGGTTTGTCGCTCA TTCTT-3') and *ppp2r2c* (5'-GGTGCTCTCGCCGTC CTCACCCATC-3') MOs targeting the transcriptional initiation ATG of *terfa* (*terfa* MO) and *ppp2r2c* (*ppp2r2c* MO) were obtained from Gene Tools. The sequence of control MO which had no target and significant biological function was TCCACACAGTGGTTCAAATCCCA CAT. The powder was diluted with sterile water and stored at room temperature. The full-length capped mRNA samples were all synthesized from linearized plasmids using the mMessage mMachine SP6 kit (Invitrogen, Thermo Fisher, USA). The microinjection concentration of *ppp2r2c* MO and *ppp2r2c* mRNA was 0.1 mmol/L and 20 ng/μL, respectively, while the microinjection concentration of *terfa* MO and *terfa* mRNA were as described previously [12]. The morpholino and mRNA were microinjected into embryos at one-cell stage with an IM-300 microinjector system (Narishige Scientific Instrument Laboratory, Tokyo, Japan).

Immunofluorescence of zebrafish's embryo slices

The embryos were collected into 1.5 mL Eppendorf tubes at 72 h post fertilization (hpf) and fixed in 4% PFA at 4 °C overnight. The embryos were embedded in OCT compound (SAKURA) and cryosectioned into 10 μm slices. Next, embryo sections were permeabilized and blocked with 0.05% Triton X-100, 2% FBS in 1X PBS for 1 h at room temperature. Hybridization with primary antibodies was performed at 4°C overnight followed by washing three times with 0.1% Tween-20 in PBS. Hybridization with corresponding secondary antibodies (Invitrogen) was performed at 37°C for at least 2 h. Finally, the brain slices were incubated with 1X DAPI for 10 min at room temperature. Imaging was performed using a confocal laser scanning microscope (Zeiss 880). The antibodies used in this study are listed in Supplementary Table 1.

Statistical analysis

Statistical analyses were performed using GraphPad Prism version 9.0 (GraphPad Software, Boston, MA, USA). The normality of the data was assessed with the Shapiro-Wilk test. For normally distributed data from at least 3 independent experiments, the unpaired two-tailed t-test was used for two-group comparisons, and one-way or two-way ANOVA with Bonferroni's post hoc test for multiple groups. For data not normally distributed, the Mann-Whitney U test was used for two-group comparisons and the Kruskal-Wallis test with Dunn's correction was employed for multiple groups. Statistical significance was set at $p < 0.05$, with specific levels indicated as follows: *p < 0.05, **p < 0.01, ***p < 0.001, ****p < 0.0001.

RESULTS

TRF2 positively regulates PPP2R2C expression and phosphatase activity of PP2A

Since we have previously shown that the downregulation of TRF2 in zebrafish embryos repressed the expression of

ppp2r2c [12, 13, 19] and PPP2R2C expression is high in neural cells, we downregulated TRF2 in both U87-MG human glioblastoma cells and SH-SY5Y human neuroblastoma cells (Fig. 1A and Supplementary Fig. 1A). In both situations, the expression of PPP2R2C was reduced. Conversely, tetracycline (TC)-induced overexpression of TRF2 in A375 cells led to PPP2R2C overexpression in a TC concentration- and time-dependent manner (Fig. 1B, 1C and Supplementary Fig. 1B-1E). Moreover, the splicing variants of *PPP2R2C* positively correlate with the TRF2 level, whether upon TRF2 downregulation or overexpression (Supplementary Fig. 1G-1I). Therefore, the regulation of PPP2R2C by TRF2 is conserved among vertebrates. Interestingly, TRF2 specifically regulated *PPP2R2C* among the PP2A B55 subunits (*PPP2R2A, PPP2R2B, PPP2R2C, PPP2R2D*; Fig. 1D and Supplementary Fig. 1F).

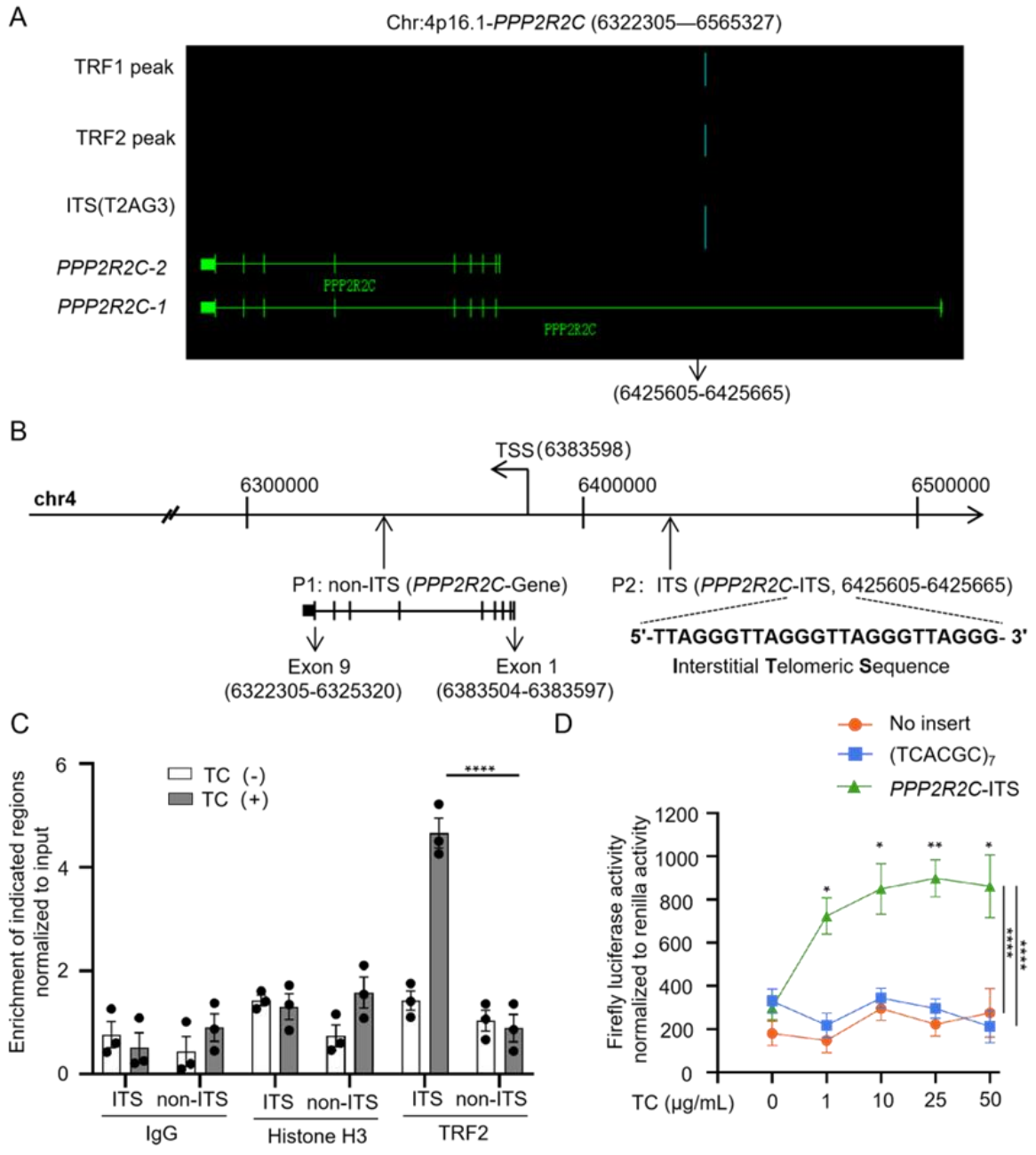

Figure 2. TRF2 Binds to and Transactivates the Interstitial Telomeric Sequence (ITS) of *PPP2R2C*. (A) Schematic diagram illustrating TRF2-binding sites within the *PPP2R2C* gene locus, generated following re-analysis of chromatin immunoprecipitation sequencing (ChIP-Seq) data [13]. In the diagram, TRF1 peaks, TRF2 peaks, and interstitial telomeric sites (ITS) are explicitly indicated. **(B)** Schematic representation of the exact chromosomal localization of ITS sites and the

PPP2R2C gene region on chromosome 4. The arrow denotes the transcription start site (TSS) of the *PPP2R2C* gene. Primers labeled P1 and P2 correspond to those used in the ChIP-quantitative PCR (qPCR) experiment described in panel (C). **(C)** ChIP assays were performed using anti-TRF2 antibody or anti-Histone H3 antibody in A375 cells. Prior to ChIP, cells were treated with tetracycline (TC, 50 μg/mL) for 12 hours to induce TRF2 overexpression. Immunoprecipitated DNA was purified and subjected to qPCR analysis. Data are presented as the fold enrichment of TRF2 binding at the *PPP2R2C* ITS region (amplified by primer P2) or non-ITS regions (amplified by primer P1), with normalization to input DNA (n = 3; ****p < 0.0001; statistical analysis performed using two-way analysis of variance [ANOVA] followed by Bonferroni's post hoc test). **(D)** Luciferase reporter assays were conducted in A375 cells. Cells were first transfected with the indicated luciferase reporter constructs and cultured for 36 hours; subsequently, cells were also treated with TC at the indicated concentrations for 12 hours to induce TRF2 overexpression. A Renilla luciferase plasmid was co-transfected as an internal control to normalize for transfection efficiency. The $(TCACGC)_7$ sequence served as a non-specific repetitive sequence control, with the same number of repeats as the ITS of the *PPP2R2C* gene. Data represent the quantification of three independent experimental replicates. Statistical analyses were performed using two-way ANOVA followed by Bonferroni's post hoc test (*p < 0.05, **p < 0.01, ****p < 0.0001).

Since PPP2R2C positively regulates PP2A phosphatase activity through counteracting phosphorylation of the C subunit of PP2A (PPP2CA) at Tyr 307 [18], we further explored the effect of TRF2 on PP2A phosphatase activity and the mechanism through which TRF2 regulates PP2A activity. After upregulation of TRF2, we observed increased PP2A phosphatase activity, while knocking down of TRF2 decreased PP2A phosphatase activity (Fig. 1E). Parallel to PPP2R2C, overexpression of TRF2 led to decreased phosphorylation of PPP2CA at Tyr 307 while downregulation of TRF2 had the opposite effect (Fig. 1F).

In summary, TRF2 positively regulates the expression of PPP2R2C and increases the activity of PP2A.

TRF2 binds to and transactivates the ITS of *PPP2R2C*

The human *PPP2R2C* gene contains an ITS bound by TRF1 and TRF2 as previously found by Chromatin Immunoprecipitation (ChIP) [13] (Fig. 2A and 2B), a result confirmed here for TRF2 (Fig. 2C). In contrast to TRF2, TRF1 and RAP1 downregulation do not impact *PPP2R2C* expression, suggesting that TRF2 exerts a specific effect on *PPP2R2C* expression (Supplementary Fig. 2). We therefore asked whether the binding of TRF2 to the intronic ITS of *PPP2R2C* has transactivation properties. Indeed, luciferase reporter analysis demonstrated that TRF2 has transactivating activities dependent on the presence of the ITS of *PPP2R2C* (Fig. 2D).

PPP2R2C and TRF2 act in the same pathway of DDR attenuation

Given that PP2A is involved in DNA damage repair by dephosphorylating γ-H2AX [21] and PPP2R2C positively regulates the activity of PP2A [18], we explored whether PPP2R2C inhibits DDR. Treatment with zeocin, a radiomimetic agent that induces random DNA double-strand breaks (DSBs) [22], activated the DDR as evidenced by concentration-dependent γ-H2AX accumulation (Fig. 3A). Notably, γ-H2AX levels increased further upon PPP2R2C knockdown or inhibition of PP2A activity with okadaic acid (OA) in zeocin-treated cells (Fig. 3A and Supplementary Fig. 3A). We next validated these findings using etoposide (VP-16), which induces DNA damage by stabilizing topoisomerase II-DNA cleavage complexes [23]. In SH-SY5Y cells, PPP2R2C downregulation exacerbated VP-16-induced DNA damage, whereas PPP2R2C overexpression alleviated DNA damage upon DNA damage stress (Supplementary Fig. 3B).

Besides, comet assays revealed that DNA damage in SH-SY5Y cells peaked immediately following VP-16 treatment (0 h) and returned to baseline levels 6 h post VP-16 treatment (Fig. 3B). PPP2R2C downregulation contributed to DNA damage that was exacerbated during the DNA damage repair process in the comet assay (Fig. 3B). On the contrary, PPP2R2C overexpression markedly attenuated DNA damage during the DNA damage repair process (Fig. 3C). Taken together, we concluded that PPP2R2C protects against DNA damage response.

Since TRF2 inhibits DDR activation through ATM pathways, we wondered whether TRF2 inhibited DDR through the upregulation of PPP2R2C. As expected, VP-16 successfully induced DNA damage and ATM pathway activation (Supplementary Fig. 3C). Moreover, upregulation of TRF2 resulted in γ-H2AX and phosphorylated form of ATM (p-ATM) reduction (Supplementary Fig. 3C). Besides, DNA damage triggered by TRF2 or PPP2R2C downregulation was not aggravated by further PPP2R2C or TRF2 inhibition. However, overexpression of PPP2R2C partially rescued DNA damage caused by TRF2 inhibition (Fig. 3D, 3E and Supplementary Fig. 3D).

The loss of TRF2 led to senescence when unrepaired DNA damage accumulated [24]. In accordance with TRF2, inhibition of PPP2R2C in MRC-5 primary fibroblast cells led to premature senescence as revealed by increased SA-β-galactosidase staining (Supplementary Fig. 3E). We conclude that TRF2 upregulates the expression of PPP2R2C, whose protein product functions

to attenuate DDR, most likely as part of the PP2A heterotrimeric phosphatase.

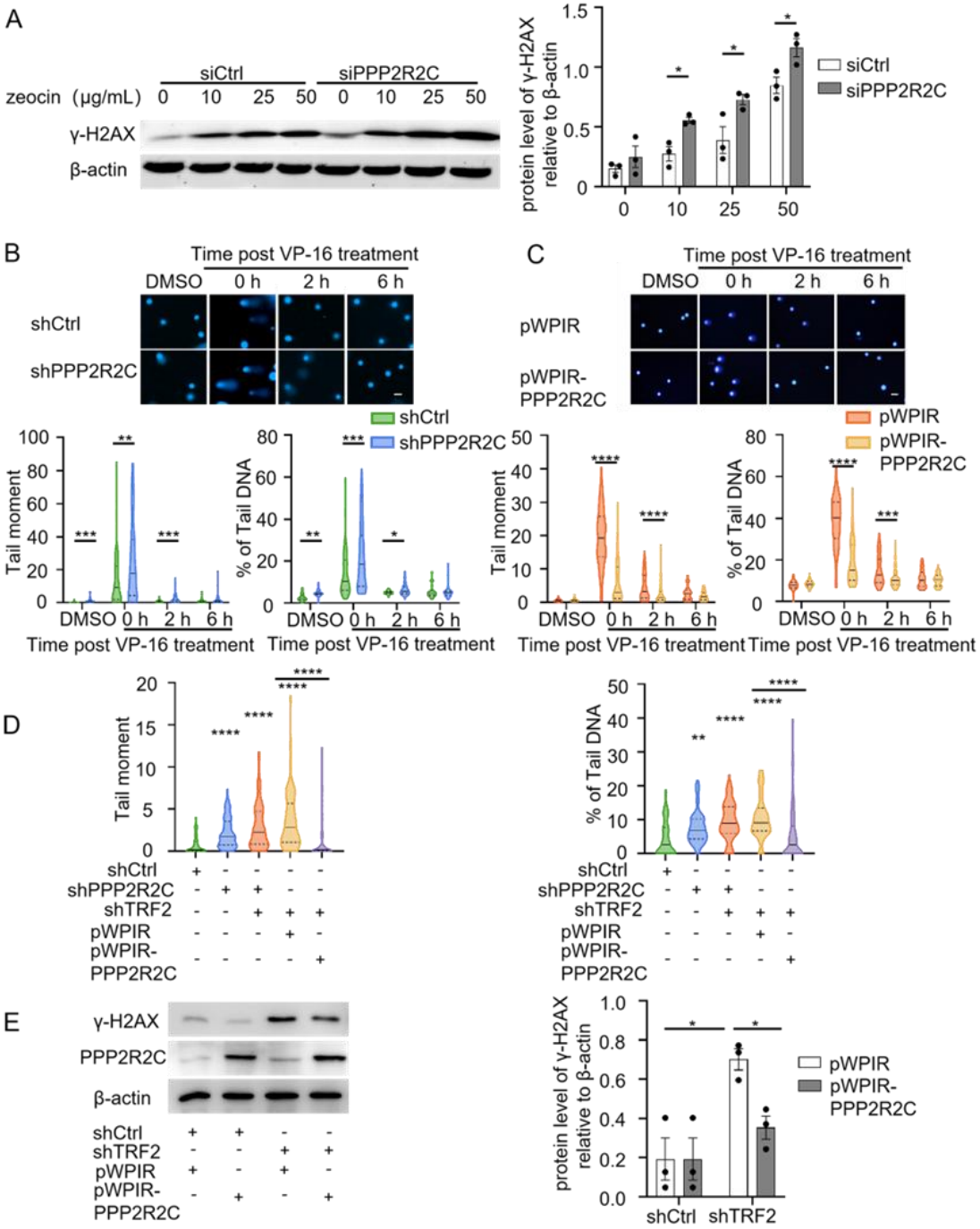

Figure 3. PPP2R2C and TRF2 Act in the Same Pathway of DNA Damage Response (DDR) Attenuation. (A) WB analysis was performed to detect the protein level of γ-H2AX in MRC-5 cells. The experimental workflow was as follows: cells were first transfected with siRNA targeting PPP2R2C (siPPP2R2C) or a scramble siRNA (siCtrl) and cultured for 48 hours; subsequently, cells were treated with zeocin at the indicated concentrations for 24 hours. Band intensities of γ-H2AX were quantified via grayscale analysis and normalized to β-actin (internal reference) (n = 3; *p < 0.05; statistical analysis performed using two-way analysis of variance [ANOVA] followed by Bonferroni's post hoc test). **(B)** Comet assay was conducted to evaluate DNA damage levels in SH-SY5Y cells under the indicated experimental conditions. Cells were treated with etoposide (VP-16, 5 μg/mL) for 1 hour to induce DNA damage, then harvested at the indicated time points post-treatment. Two key parameters of the comet assay—tail moment and tail DNA percentage—were quantified for statistical analysis. Truncated violin plots depict DNA damage levels under the indicated conditions as assessed by comet assay. Depicted are mean (solid line) and 25th/75th quartiles (dotted lines). The number of cells analyzed per group was 87, 44, 100,

86, 31, 75, 20, and 51, respectively (*p < 0.05, **p < 0.01, ***p < 0.001; statistical analyses performed using the Kruskal-Wallis test with Dunn's correction). Scale bars: 20 μm. **(C)** Truncated violin plots depict DNA damage levels in SH-SY5Y cells via comet assay following the indicated treatments. Cells were treated with VP-16 (10 μg/mL) for 1 hour to induce DNA damage. Tail moment and tail DNA percentage were quantified to characterize DNA damage severity. The number of cells analyzed per group was 85, 64, 58, 42, 70, 105, 51, and 79, respectively (***p < 0.001, ****p < 0.0001; statistical analyses conducted using the Kruskal-Wallis test with Dunn's correction). Scale bars: 20 μm. **(D)** Truncated violin plots depict DNA damage levels in SH-SY5Y cells via comet assay under the indicated experimental conditions. Dashed Line: median of data. Dotted Line: Quartiles of Data. Tail moment and tail DNA percentage were quantified to evaluate DNA damage levels. The number of cells analyzed per group was 70, 88, 93, 59, and 122, respectively (**p < 0.01, ****p < 0.0001; statistical analyses performed using the Kruskal-Wallis test with Dunn's correction). Scale bars: 20 μm. **(E)** WB analysis was carried out to detect the protein levels of γ-H2AX and PPP2R2C in SH-SY5Y cells. The experimental procedure was as follows: cells were first infected with lentiviruses encoding scramble shRNA (shCtrl) or TRF2-targeting shRNA (shTRF2); after establishing stable knockdown, cells were further transfected with lentiviruses expressing either the empty vector (pWPIR) or the PPP2R2C-overexpressing vector (pWPIR-PPP2R2C). Band intensities of γ-H2AX and PPP2R2C were quantified via grayscale analysis and normalized to β-actin (n = 3; *p < 0.05; statistical analysis performed using the two-way ANOVA followed by Bonferroni's post hoc test).

PPP2R2C specifically protects telomeres and pericentromeres during S phase

Next, we explored whether PPP2R2C had protective roles against DNA damage at the two difficult to replicate regions that require TRF2 to prevent DNA damage: telomeres and pericentromeres. To this purpose, we assayed DDR activation by the combination of the immunostaining of the DDR factors 53BP1 and γ-H2AX with specific peptide nucleic acid (PNA) probing to score the colocalization at telomeres, pericentromeres, and centromeres, also known as TIF (telomere dysfunction-induced foci), PIF (pericentromere dysfunction-induced foci) and CIF (centromere dysfunction-induced foci), respectively [11]. In different cell types, knocking-down PPP2R2C led to an increase of TIFs and PIFs but not CIFs (Fig. 4A, 4B and Supplementary Fig. 4A-4E) indicating that PPP2R2C protected against DNA damage at telomeres and pericentromeres, but not centromeres, in striking agreement with the role of TRF2 at these three regions [11]. The number of TIFs and PIFs increased significantly in S phase and upon replicative stress in PPP2R2C compromised cells (Fig. 4C, 4D and Supplementary Fig. 4F-4H), indicating that the protective role of PPP2R2C is linked to DNA replication. Then, we analyzed p-ATM and RPA as markers of the ATM and ATR pathways, respectively. Knocking-down PPP2R2C led to a combined activation of p-ATM and RPA at telomeres and pericentromeres in S phase and upon replicative stress (Supplementary Fig. 4I and 4J). Taken together, these results indicate that PPP2R2C protects telomeres and pericentromeres during S phase from DNA damage activating both the ATM and ATR pathways as previously shown for replicative stress [25].

PPP2R2C colocalizes with TRF2 during S phase

Next, we assayed by confocal microscopy whether, in addition to being upregulated by TRF2, PPP2R2C can colocalize with TRF2. In synchronized SH-SY5Y cells by two pulses of thymidine [26], PPP2R2C colocalized with TRF2, as detected by Proximity Ligation Assay (PLA), with a peak of colocalization in S phase (Fig. 5A). This colocalization with TRF2 was also observed in human MRC-5 and 293T cells (Supplementary Fig. 5B-5D). This preferential colocalization of PPP2R2C and TRF2 in S phase was confirmed in non-synchronized cells by EdU staining, in cells treated with the dNTP synthesis inhibitors hydroxyurea (HU) and aphidicolin for 24 h [11] by confocal colocalization of PPP2R2C with TRF2 (Fig. 5B, 5C and Supplementary Fig. 5E). Combination of HU and aphidicolin leads to a significant increase in the number of RPA foci compared to either agent alone (Supplementary Fig. 5G), consistent with flow cytometry data demonstrating successful replication stress induction and enhanced stress levels in the combination group (Supplementary Fig. 5H).

Since TRF2 can be localized at both telomeres and pericentromeres, we asked whether PPP2R2C is localized at these two regions. Given that PPP2R2C is highly expressed in neural cells, we extracted primary glial cells from the brain of wild-type mice 24 h after birth and carried out transfection after one week of culture. In these primary cells, PPP2R2C colocalized with telomeres as revealed by a PNA probe (Supplementary Fig. 5A). In human cells, we found that PPP2R2C can also be localized to pericentromeres as probed with a SatIII PNA (pericentromeric satellite DNA repeats) and this is increased during replication and replicative stress (Fig. 5D and Supplementary Fig. 5F). On the contrary, replicative stress did not lead to the association of PPP2R2C with centromeres, showing the specificity of the association of PPP2R2C with telomeres and pericentromeres during replication (Supplementary Fig. 5I). The nature of the association of PPP2R2C with TRF2 and whether this association involves the entire PP2A phosphatase are unknown.

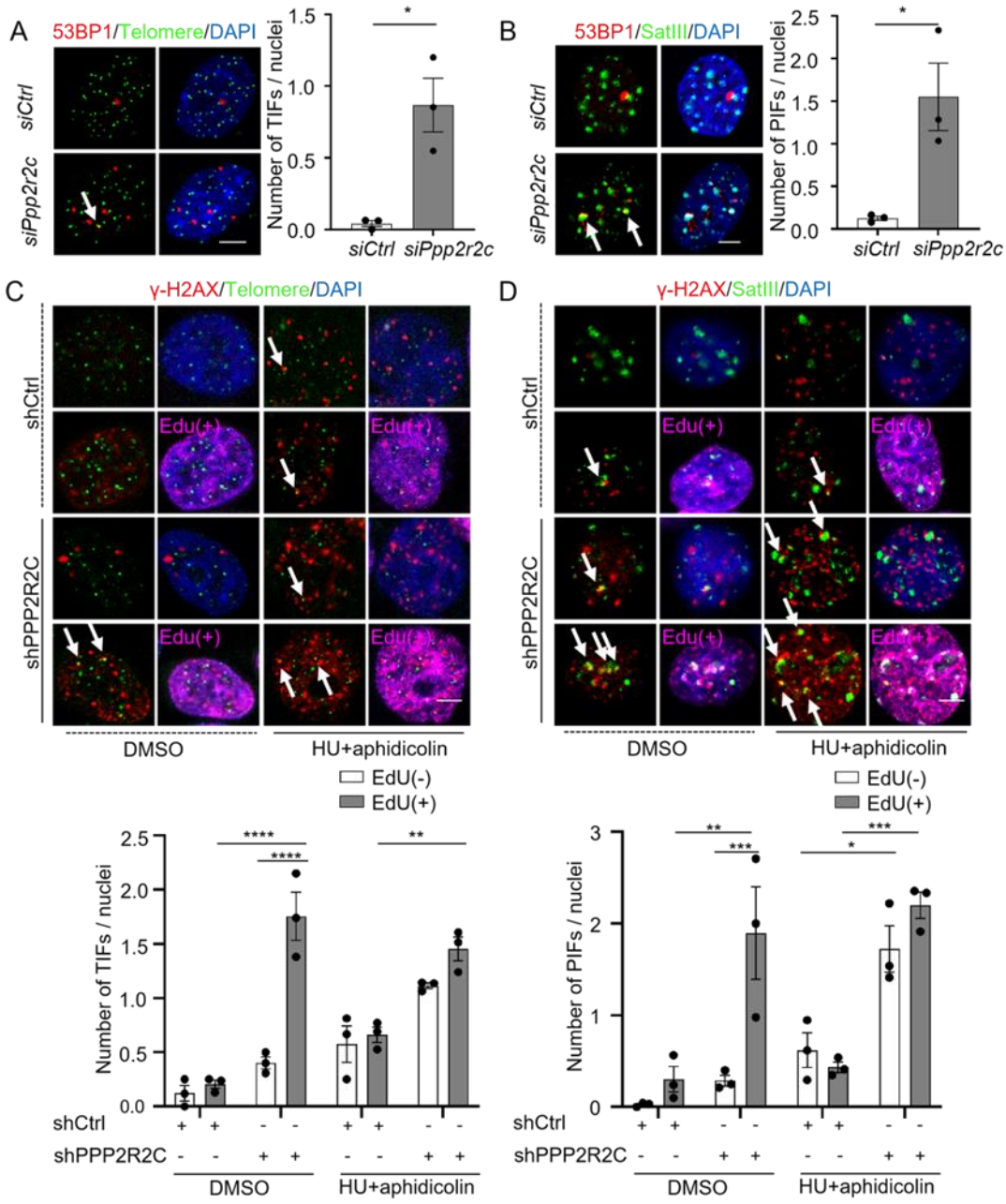

Figure 4. PPP2R2C Specifically Protects Telomeres and Pericentromeres during S phase. (A-B) Immunofluorescence (IF) staining was performed to detect 53BP1 foci (red), combined with fluorescence in situ hybridization (FISH) using probes targeting telomeres (to identify telomere dysfunction-induced foci, TIF; panel A) or SatIII (to identify pericentromere dysfunction-induced foci, PIF; panel B) (both labeled green). These analyses were conducted in primary glial cells isolated from the brains of newborn wild-type mice. Prior to staining, cells were transfected with the indicated siRNAs and cultured for 72 hours. Scale bar: 5 μm. Quantification of TIFs (panel A) and PIFs (panel B) was performed, with n=3 biological replicates and 30 cells analyzed per experimental condition (*$p < 0.05$; statistical analysis conducted using the two-tailed t-tests). **(C-D)** Confocal microscopy was used to capture representative images of TIFs (panel C) and PIFs (panel D) in 293T cells with stable PPP2R2C knockdown (via transduction with shPPP2R2C). For S phase cell labeling, cells were incubated with 5-ethynyl-2'-deoxyuridine (EdU, 10 μM) for 2 hours. Additionally, cells were treated with DMSO or a combination of hydroxyurea (HU, 1.5 μM) and aphidicolin (300 nM) for 24 hours. Scale bar: 5 μm. Quantification of TIFs (panel C) and PIFs (panel D) per nuclei was performed. Data are presented as mean ± SEM from three biological replicates. Statistical analyses were performed using the two-way ANOVA followed by Bonferroni's post hoc test (*$p < 0.05$, **$p < 0.01$, ***$p < 0.001$, ****$p < 0.0001$).

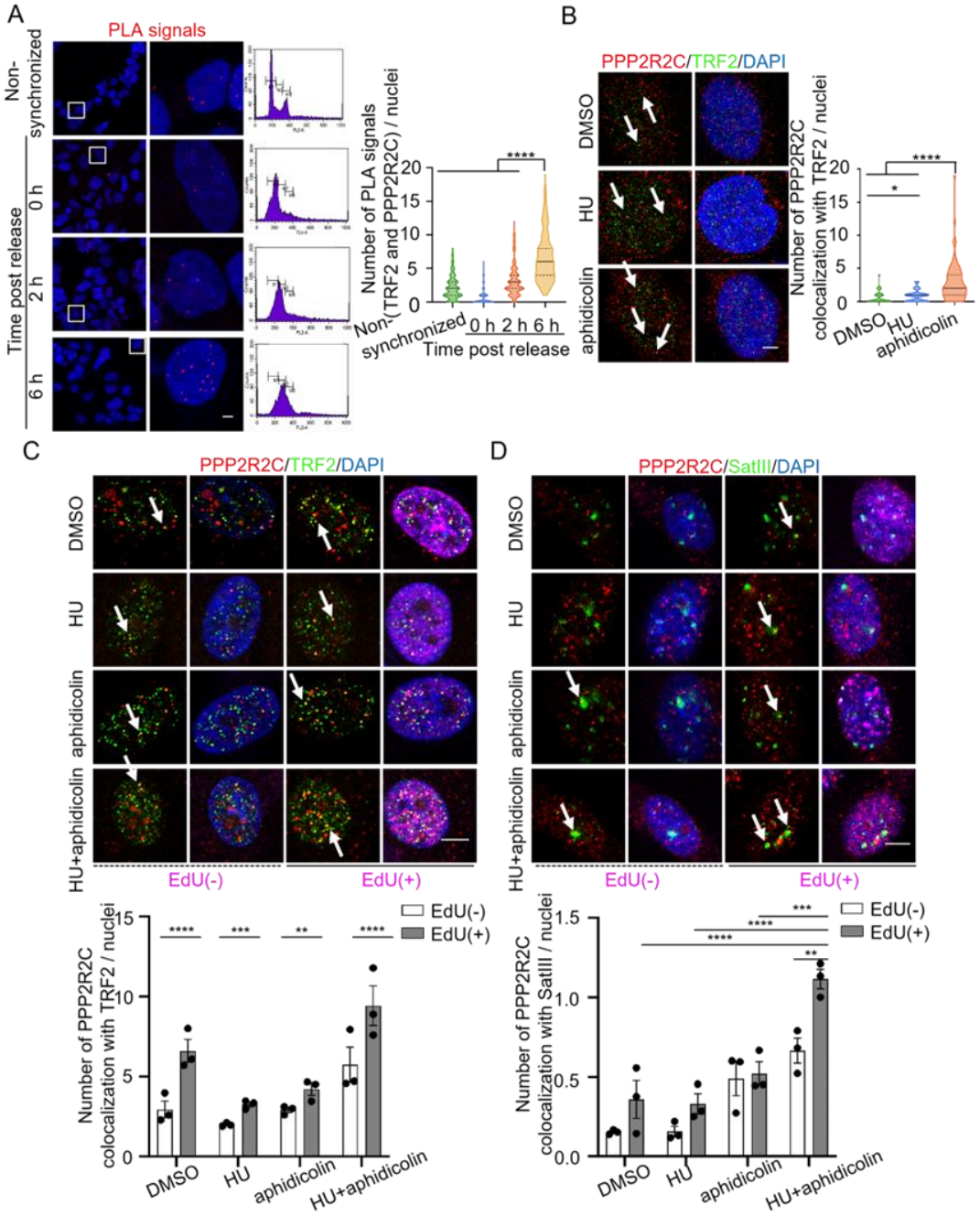

Figure 5. PPP2R2C is Recruited to Telomeres and Pericentromeres during S phase. (A) Proximity ligation assay (PLA) was performed to detect in situ protein-protein interactions between TRF2 and PPP2R2C in thymidine-synchronized SH-SY5Y cells under the indicated experimental conditions; positive PLA signals (representing TRF2-PPP2R2C interactions) are shown in representative projected images of confocal sections. Insets display enlarged regions of interest (outlined by white boxes). Scale bar: 20 μm. A fluorescence-activated cell sorting (FACS) analysis is included to verify the cell cycle progression of synchronized cells. Truncated violin plots depict PLA signals per nuclei, with n = 2 biological replicates and 70 cells analyzed per experimental condition. Dashed Line: median of data. Dotted Line: Quartiles of Data. **(B)** Confocal microscopy was used to capture representative images of colocalization between PPP2R2C (stained red) and TRF2 (stained green) in SH-SY5Y cells. Cells were treated with DMSO, hydroxyurea (HU, 1.5 μM) for 24 hours, or aphidicolin (300 nM) for 24 hours. Scale bar: 5 μm. Truncated violin plots depict PPP2R2C-TRF2 colocalization events, with 66 cells analyzed for the DMSO group, 44 cells for the HU group, and 74 cells for the aphidicolin group. **(C-D)** Representative images of confocal microscopy were used to capture representative images of PPP2R2C (stained red) colocalized with TRF2 (stained green, panel C) or SatIII (stained green, panel D) in U87-MG

cells. For S-phase cell labeling, cells were incubated with 5-ethynyl-2'-deoxyuridine (EdU, 10 μM) for 2 hours; cells were also treated with DMSO, HU (1.5 μM, 24 hours), aphidicolin (300 nM, 24 hours), or combination of HU and aphidicolin. Scale bar: 5 μm. Quantification of PPP2R2C-TRF2 colocalization events (panel C) and PPP2R2C-SatIII colocalization events (panel D) was conducted, with n = 3 biological replicates and 40 cells analyzed per experimental condition. Kruskal-Wallis test with Dunn's correction for (A), and (B), two-way ANOVA followed by Bonferroni's post hoc test for (C), and (D), *p < 0.05, **p < 0.01, ***p < 0.001, ****p < 0.0001.

TRF2-PPP2R2C axis plays an important role in maintaining normal neurodevelopment in zebrafish

Finally, we investigated the role of the PPP2R2C-TRF2 axis *in vivo*. Our previous results have shown that fish compromised for *terfa* (the homolog of human *TRF2* gene in zebrafish) exhibited a prominent and specific embryonic neurodevelopmental failure [19]. This, together with the neural specificity of PPP2R2C expression [17], led us to examine the effect of PPP2R2C inhibition on zebrafish development.

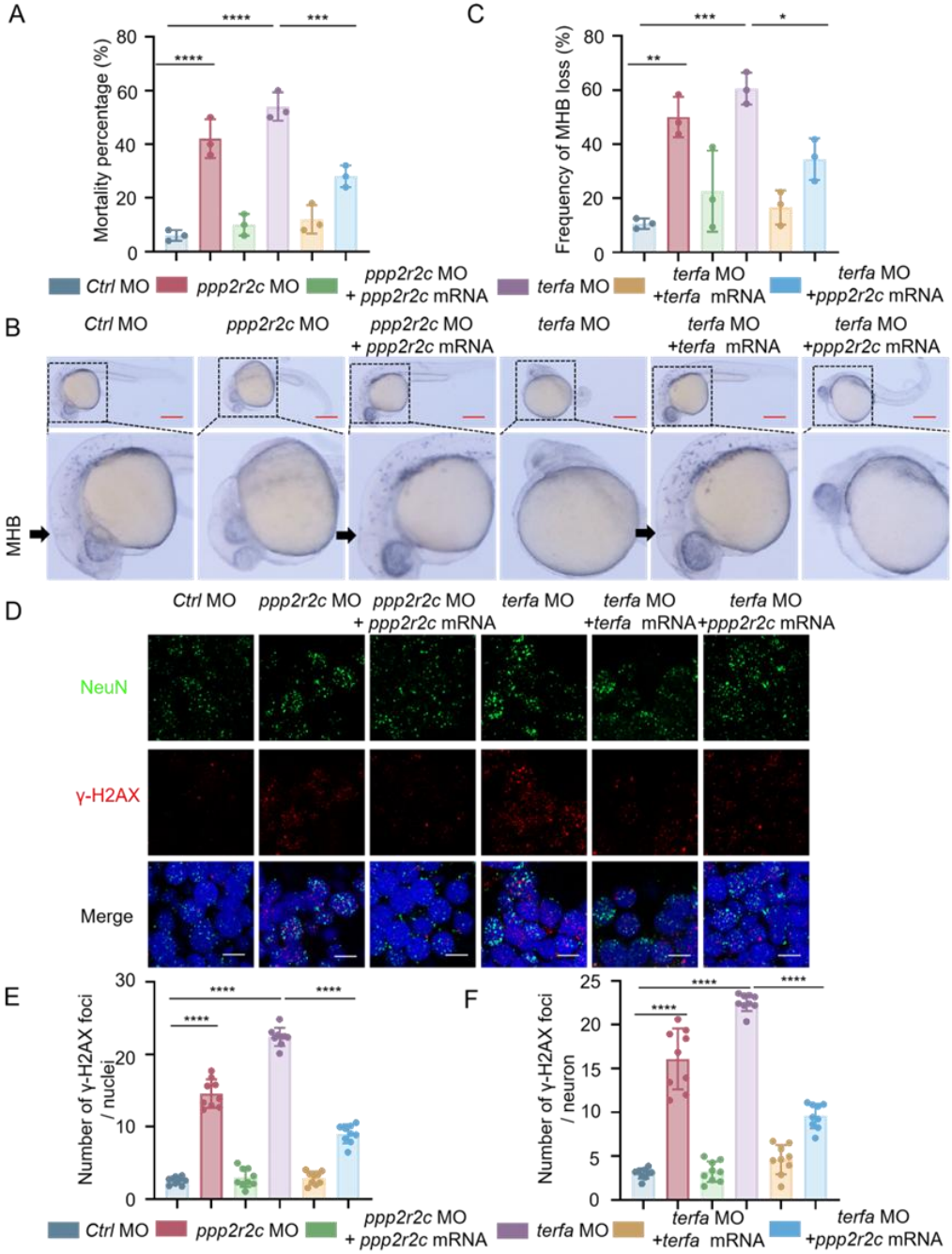

Figure 6. PPP2R2C Plays an Important Role in Maintaining Neurodevelopment in Zebrafish. (A) Tu wild-type zebrafish embryos were microinjected with the indicated morpholino antisense oligonucleotides (MOs) or messenger RNAs (mRNAs). The mortality percentage of the embryos was calculated at 24 hours post fertilization (hpf). **(B-C)** Representative lateral views of the midbrain–hindbrain boundary (MHB) in Tu wild-type zebrafish larvae (microinjected with the indicated MOs or mRNAs) were captured via light microscopy at 24 hpf. Scale bar: 20 μm. Quantification of the frequency of MHB loss was performed for these larvae to evaluate MHB development defects. **(D)** Tu wild-type zebrafish embryos were microinjected with the indicated MOs or mRNAs. At 72 hours post-fertilization (hpf), confocal microscopy was used to capture representative images of the hindbrain region. Double immunofluorescence staining was performed to label NeuN (green) and γ-H2AX (red). Scale bars: 5 μm. **(E-F)** Tu wild-type zebrafish embryos were microinjected with the indicated MOs or mRNAs, and at 72 hpf, the hindbrain regions were analyzed: (E) Quantification of the γ-H2AX foci per nuclei; (F) Quantification of γ-H2AX foci per neuronal nuclei (neuronal nuclei were identified via NeuN staining, a specific neuronal marker). For both analyses, n = 3 biological replicates, 9 fish per group and over 30 nuclei were analyzed per fish. All data are presented as mean ± SEM of three biological replicates. Statistical analyses were performed using one-way analysis of variance [ANOVA] followed by Bonferroni's post hoc test, with significance indicated as follows: *$p < 0.05$, **$p < 0.01$, ***$p < 0.001$, ****$p < 0.0001$.

Specifically, we assessed the effect of PPP2R2C inhibition on early embryonic development by antisense oligonucleotide morpholino (MO) against *ppp2r2c* (*ppp2r2c* MO). Microinjection of *ppp2r2c* MO resulted in 40% embryonic mortality at 24 h post fertilization (hpf) and the mortality was higher than control (Fig. 6A). Surviving embryos displayed central nervous system abnormalities characterized by mid-hindbrain boundary (MHB) loss (Fig. 6B and 6C). Importantly, *terfa* inhibition led to increased embryonic mortality and MHB loss which could be partially rescued by exogenously overexpressing *ppp2r2c* (Fig. 6A-6C). We ruled out an off target of the MO against *terfa* by showing a rescue of *ppp2r2c* expression upon co-injection of *terfa* mRNA (Supplementary Fig. 6A and 6B).

Besides, the *terfa* or *ppp2r2c*-compromised fish at 72 hpf exhibited a premature-aging phenotype including spinal curvature (Supplementary Fig. 6C and 6D). Therefore, we investigated the protective role of PPP2R2C in DNA damage response in zebrafish. Quantitative analysis revealed elevated DNA damage signaling in *ppp2r2c*-compromised (72 hpf) brain tissue, with a significantly higher number of γ-H2AX foci in the hindbrain nuclei (Fig. 6D and 6E). Moreover, DNA damage induced by TRF2 inhibition was partially rescued by PPP2R2C expression restoration (Fig. 6D and 6E). Specifically, quantification of γ-H2AX foci number in individual neurons showed consistent trends across other cell types, indicating that the protective effect of PPP2R2C is not restricted to neurons (Fig. 6D and 6F). Notably, this partial rescue in zebrafish precisely supports our model that TRF2 regulates neural development through multiple downstream pathways, including *ppp2r2c* and *snap25* [19]. Therefore, overexpressing *ppp2r2c* alone is not expected to fully compensate for the loss of *terfa*, which aligns with the in vivo complexity.

Collectively, these results demonstrate that PPP2R2C plays an important role in protecting against unwanted DDR activation and maintaining development of the central nervous system as a downstream effector of TRF2.

DISCUSSION

The important finding of this study is the discovery of a new mechanism by which TRF2 protects against DNA damage involving the transcriptional upregulation of PPP2R2C encoding a regulatory subunit of the phosphatase PP2A, a key regulator in the DDR and repair [27]. Indeed, PP2A directly promotes dephosphorylation of γ-H2AX [21] and replication protein A (RPA) [28].

This function of TRF2 is accomplished in human cells, at least in part, by the binding of TRF2 to an intronic ITS of *PPP2R2C* that confers transactivating activities to this ITS. Moreover, we reveal that PPP2R2C, and likely PP2A, are associated with telomeres and pericentromeres during replication and during replication stress — two difficult-to-replicate regions that require TRF2 for a smooth progression of the replication fork. The positive proximity ligation assay (PLA) signal confirms the spatial proximity between TRF2 and PPP2R2C, suggesting that this proximity is mediated by their respective functional complexes: the shelterin complex for TRF2 and the PP2A holoenzyme for PPP2R2C. The precise molecular nature of the association between PPP2R2C and these genomic loci (telomeres and pericentromeres) remains to be fully elucidated.

Different from other regulatory subunits of phosphatase PP2A, PPP2R2C is highly expressed in the nervous system [29, 30]. We found here that the inhibition of PPP2R2C in zebrafish embryos leads to neurodevelopmental abnormalities and DNA damage in neural cells. This result, together with the downregulation of PPP2R2C and PP2A activity in aging brains of wild-type mice or zebrafish [17, 18] as well as in mouse models of Alzheimer's disease [18], suggests that the TRF2-PPP2R2C axis acting against replicative damage is

prominent to allow proper division of neural or progenitor cells, therefore representing an interesting target for innovative therapies of neurodegenerative diseases.

Limitations

We acknowledge that the use of diverse cell lines could be perceived as a limitation. However, we believe it also serves as a strength, as it demonstrates the core function of the TRF2-PPP2R2C pathway across multiple relevant biological contexts, thereby enhancing the robustness and potential universality of our findings. Future studies will focus on validating these mechanisms into more unified neuronal models. Nevertheless, the lack of a unified strategy for DNA damage assessment, which involves the use of variable cell lines and genotoxic agents, remains a limitation. Confirming these findings under standardized conditions is a key future objective.

Acknowledgements

Work in the JY/YML laboratories was supported by the National Natural Science Foundation of China (grant numbers 82225018, 81971312, 91749126, 81911530241, 92149302, 81871549, and 81671900), the Program of Shanghai Academic/Technology Research Leader (grant number 19XD1422500), and the Shanghai Municipal Education Commission (Oriental Scholars Program, 2019). Work in the EG laboratory was supported by the Foundation ARC, the ANR grant TELOPOST, and the Inserm cross-cutting program AGEMED. The work was also supported by the French Government (National Research Agency, ANR) through the "Investments for the Future" LABEX SIGNALIFE program (reference ANR-11-LABX-002801).

Author contributions

Jing Ye and Eric Gilson designed the experiments. Xiuyun Zhai, Cuicui Wang, Yilin Ying, Waiian Leong, Lianxiang Chen, Bohua Wei, Xiaojiao Cheng, Sheng Huang, Qiaowen Chen performed the experiments. Jing Ye, Yiming Lu, and Eric Gilson analyzed the data. Jing Ye and Eric Gilson wrote the paper.

Competing interests

The authors declare that they have no conflict of interest.

Data and materials availability

All data and information relevant to this study are available from the corresponding author upon reasonable request.

Supplementary Materials

The Supplementary data can be found online at: www.aginganddisease.org/EN/10.14336/AD.2025.1249.

References

[1] Cech TR (2004). Beginning to understand the end of the chromosome. Cell, 116:273-279.

[2] Palm W, de Lange T (2008). How shelterin protects mammalian telomeres. Annu Rev Genet, 42:301-334.

[3] Benarroch-Popivker D, Pisano S, Mendez-Bermudez A, Lototska L, Kaur P, Bauwens S, et al. (2016). TRF2-Mediated Control of Telomere DNA Topology as a Mechanism for Chromosome-End Protection. Mol Cell, 61:274-286.

[4] Doksani Y, Wu JY, de Lange T, Zhuang X (2013). Super-resolution fluorescence imaging of telomeres reveals TRF2-dependent T-loop formation. Cell, 155:345-356.

[5] Griffith JD, Comeau L, Rosenfield S, Stansel RM, Bianchi A, Moss H, et al. (1999). Mammalian telomeres end in a large duplex loop. Cell, 97:503-514.

[6] Sarek G, Kotsantis P, Ruis P, Van Ly D, Margalef P, Borel V, et al. (2019). CDK phosphorylation of TRF2 controls t-loop dynamics during the cell cycle. Nature, 575:523-527.

[7] Amiard S, Doudeau M, Pinte S, Poulet A, Lenain C, Faivre-Moskalenko C, et al. (2007). A topological mechanism for TRF2-enhanced strand invasion. Nat Struct Mol Biol, 14:147-154.

[8] van Overbeek M, de Lange T (2006). Apollo, an Artemis-related nuclease, interacts with TRF2 and protects human telomeres in S phase. Curr Biol, 16:1295-1302.

[9] Lenain C, Bauwens S, Amiard S, Brunori M, Giraud-Panis MJ, Gilson E (2006). The Apollo 5' exonuclease functions together with TRF2 to protect telomeres from DNA repair. Curr Biol, 16:1303-1310.

[10] Ye J, Lenain C, Bauwens S, Rizzo A, Saint-Léger A, Poulet A, et al. (2010). TRF2 and apollo cooperate with topoisomerase 2alpha to protect human telomeres from replicative damage. Cell, 142:230-242.

[11] Mendez-Bermudez A, Lototska L, Bauwens S, Giraud-Panis MJ, Croce O, Jamet K, et al. (2018). Genome-wide Control of Heterochromatin Replication by the Telomere Capping Protein TRF2. Mol Cell, 70:449-461.e445.

[12] Wagner KD, Ying Y, Leong W, Jiang J, Hu X, Chen Y, et al. (2017). The differential spatiotemporal expression pattern of shelterin genes throughout lifespan. Aging (Albany NY), 9:1219-1232.

[13] Simonet T, Zaragosi LE, Philippe C, Lebrigand K, Schouteden C, Augereau A, et al. (2011). The human TTAGGG repeat factors 1 and 2 bind to a subset of interstitial telomeric sequences and satellite repeats. Cell Res, 21:1028-1038.

[14] Ye J, Renault VM, Jamet K, Gilson E (2014). Transcriptional outcome of telomere signalling. Nat Rev Genet, 15:491-503.

[15] Lambrecht C, Haesen D, Sents W, Ivanova E, Janssens V (2013). Structure, regulation, and pharmacological modulation of PP2A phosphatases. Methods Mol Biol, 1053:283-305.

[16] Sontag JM, Sontag E (2014). Protein phosphatase 2A dysfunction in Alzheimer's disease. Front Mol Neurosci, 7:16.

[17] Xing J, Chen K, Gao S, Pousse M, Ying Y, Wang B, et al. (2023). Protein phosphatase 2A activators reverse age-related behavioral changes by targeting neural cell senescence. Aging Cell, 22:e13780.

[18] Leong W, Xu W, Wang B, Gao S, Zhai X, Wang C, et al. (2020). PP2A subunit PPP2R2C is downregulated in the brains of Alzheimer's transgenic mice. Aging (Albany NY), 12:6880-6890.

[19] Ying Y, Hu X, Han P, Mendez-Bermudez A, Bauwens S, Eid R, et al. (2022). The non-telomeric evolutionary trajectory of TRF2 in zebrafish reveals its specific roles in neurodevelopment and aging. Nucleic Acids Res, 50:2081-2095.

[20] Kimmel CB, Ballard WW, Kimmel SR, Ullmann B, Schilling TF (1995). Stages of embryonic development of the zebrafish. Dev Dyn, 203:253-310.

[21] Chowdhury D, Keogh MC, Ishii H, Peterson CL, Buratowski S, Lieberman J (2005). gamma-H2AX dephosphorylation by protein phosphatase 2A facilitates DNA double-strand break repair. Mol Cell, 20:801-809.

[22] Mao P, Liu J, Zhang Z, Zhang H, Liu H, Gao S, et al. (2016). Homologous recombination-dependent repair of telomeric DSBs in proliferating human cells. Nat Commun, 7:12154.

[23] Deweese JE, Osheroff N (2009). The DNA cleavage reaction of topoisomerase II: wolf in sheep's clothing. Nucleic Acids Res, 37:738-748.

[24] d'Adda di Fagagna F, Reaper PM, Clay-Farrace L, Fiegler H, Carr P, Von Zglinicki T, et al. (2003). A DNA damage checkpoint response in telomere-initiated senescence. Nature, 426:194-198.

[25] Olcina MM, Foskolou IP, Anbalagan S, Senra JM, Pires IM, Jiang Y, et al. (2013). Replication stress and chromatin context link ATM activation to a role in DNA replication. Mol Cell, 52:758-766.

[26] Ge Y, Wu S, Xue Y, Tao J, Li F, Chen Y, et al. (2016). Preferential extension of short telomeres induced by low extracellular pH. Nucleic Acids Res, 44:8086-8096.

[27] Ramos F, Villoria MT, Alonso-Rodríguez E, Clemente-Blanco A (2019). Role of protein phosphatases PP1, PP2A, PP4 and Cdc14 in the DNA damage response. Cell Stress, 3:70-85.

[28] Feng J, Wakeman T, Yong S, Wu X, Kornbluth S, Wang XF (2009). Protein phosphatase 2A-dependent dephosphorylation of replication protein A is required for the repair of DNA breaks induced by replication stress. Mol Cell Biol, 29:5696-5709.

[29] DeGrande ST, Little SC, Nixon DJ, Wright P, Snyder J, Dun W, et al. (2013). Molecular mechanisms underlying cardiac protein phosphatase 2A regulation in heart. J Biol Chem, 288:1032-1046.

[30] Backx L, Vermeesch J, Pijkels E, de Ravel T, Seuntjens E, Van Esch H (2010). PPP2R2C, a gene disrupted in autosomal dominant intellectual disability. Eur J Med Genet, 53:239-243.